

First-principles study of NaAlH₄ and Na₃AlH₆ complex hydrides

A. Peles, J. A. Alford,* Zhu Ma, Li Yang, and M. Y. Chou

School of Physics, Georgia Institute of Technology, Atlanta, Georgia 30332-0430, USA

(Received 11 June 2004; published 15 October 2004)

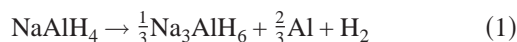
We present a first-principles investigation of the structural properties, electronic structure, and the chemical stability of the complex hydrides NaAlH₄ and Na₃AlH₆. The calculations are performed within the density functional framework employing norm conserving pseudopotentials. The structural properties of both hydrides compare well with experimental data. A detailed study of the electronic structure and the charge-density redistribution reveal the features of an ionic covalent bonding between Al and H in the (AlH₄)⁻ and (AlH₆)⁻³ anionic complexes embedded in the matrix of Na⁺ cations. The orbital hybridization and the characteristics of bonding orbitals within the complexes are identified. The calculated reaction energies of these complex hydrides are in good agreement with the experimentally determined values.

DOI: 10.1103/PhysRevB.70.165105

PACS number(s): 71.20.Ps, 61.50.Lt, 61.66.Fn

I. INTRODUCTION

Much recent research effort has been directed at investigating complex hydrides of light metals such as NaAlH₄ that are viable candidates for practical applications as hydrogen storage materials.¹⁻⁴ NaAlH₄ has a high gravimetric hydrogen capacity (5.6 wt. %) and doping with selected transition metals (Ti, Zr, Fe, etc.) is shown to speed up the rate of absorption and desorption of hydrogen under moderate conditions, making NaAlH₄ a technologically interesting material as a potential energy carrier.⁵ Unlike the traditional metal hydrides where the metal lattice is a host for hydrogen which resides in the interstitial sites, in NaAlH₄ each Al is surrounded by four H atoms, forming a metal-hydrogen complex. The dehydration process proceeds through a series of chemical reactions as follows:



and



An amount of 3.7 wt. % of hydrogen is released in the first reaction and 1.85 wt. % in the second. Further release of H₂ in the decomposition of NaH happens at very high temperature and is not considered useful for practical hydrogen storage. Understanding the fundamental physical properties of the complex hydrides involved in reversible hydrogen absorption/desorption processes is of key importance toward the design of novel materials and devices for hydrogen storage.

Here we employ first-principles approaches based on density functional theory and norm conserving pseudopotentials to conduct a comprehensive study of the structural, electronic, and stability properties of NaAlH₄ and Na₃AlH₆. Recent theoretical studies⁶⁻¹⁰ have confirmed the structural features of both complex hydrides in agreement with experimental results.¹¹⁻¹⁴ These include calculations employing the general potential linearized augmented plane-wave (LAPW) method,⁶ the projector augmented wave (PAW) method,⁷ and the pseudopotential method.⁸⁻¹⁰ The electronic structure studies for NaAlH₄ (Refs. 6-8) have suggested the

bonding picture within the complex to be either covalent⁷ or ionic.⁶ Investigations of the thermodynamic stability of complex hydrides^{8,9} have found both hydrides to be stable. In addition, the electronic structure and high-pressure phases of the lithium compounds (LiAlH₄ and Li₃AlH₆) have also been investigated using PAW and LAPW methods.¹⁵⁻¹⁷ In this work we make a systematic analysis of the electronic properties of both NaAlH₄ and Na₃AlH₆ in order to elucidate the generic bonding characteristics in complex metal hydrides. Our results suggest a covalent type of bonding between Al and H within the complex, but with a large ionicity. In contrast to previous studies, we have identified the importance of the Al *d* orbital hybridizing with the H *s* orbital in the AlH₆ complex. This explains why the BH₆ complex has never been observed, given the fact that the 3*d* state has a much higher energy than the 2*s* and 2*p* bonding states in B.

Details of the computational methodology are summarized in Sec. II. The structural properties are discussed in Sec. III. Detailed studies of the electronic structure are presented in Sec. IV and a discussion of formation energies is given in Sec. V.

II. COMPUTATIONAL METHODOLOGY

The first-principles calculations were based on density functional theory^{18,19} (DFT) with norm-conserving pseudopotentials²⁰ combined with a plane wave basis set. The pseudopotential of the Na atom was generated in the 3*s*¹3*p*⁰ configuration with the cutoff radii of 2.3 a.u.(*s*) and 2.5 a.u.(*p*). We used the partial core correction²¹ to account for the overlap of valence and core electronic states. In the case of Al we have generated pseudopotentials with and without the nonlocal *d* component from the configurations 3*s*²3*p*¹3*d*⁰ and 3*s*²3*p*¹, respectively, with following cutoff radii 1.93 a.u.(*s*), 2.43 a.u.(*p*), 2.28 a.u.(*d*).²² The pseudopotential of the H atom was constructed in the 1*s*¹ configuration with a cutoff radius of 1.25 a.u. In the calculation of the electronic structure and formation energies the generalized gradient approximation^{23,24} (GGA) to the electronic exchange-correlation energy was employed, while in the study of structural properties the local density

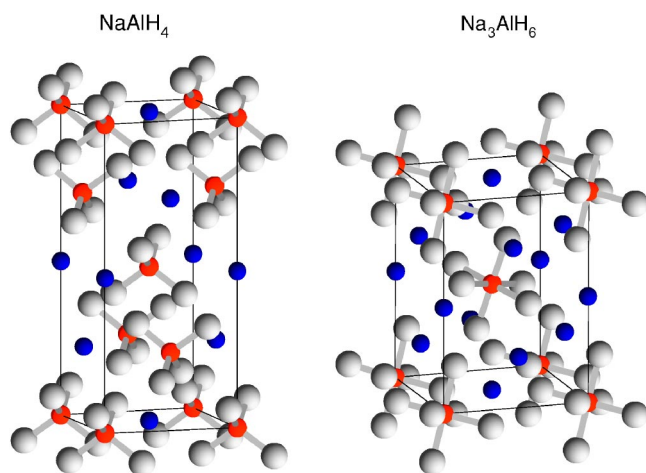


FIG. 1. (Color online) Crystal structure of tetragonal NaAlH_4 and monoclinic $\alpha\text{-Na}_3\text{AlH}_6$. Na atoms are presented by blue (dark) spheres. Tetragonal AlH_4 and octahedral AlH_6 complexes are shown with respective Al-H bonds. The central aluminum atoms are shown by small red (dark gray) spheres, while hydrogen atoms are represented by large white (light gray) spheres.

approximation²⁵ (LDA) was also considered in addition to GGA. The convergence test performed on the experimental structures of NaAlH_4 and Na_3AlH_6 yielded the choice of 55 Ry for the plane-wave energy cutoff. The Brillouin zone was sampled using a Monkhorst-Pack sampling technique,²⁶ and a shifted $4 \times 4 \times 4$ grid with 12 and 16 k points in the irreducible Brillouin zone of NaAlH_4 and Na_3AlH_6 , respectively, was found sufficient. The self-consistent total energy was converged up to 10^{-6} Ry. In order to study the thermodynamic stability of complex hydrides involved in the chemical reactions in Eqs. (1) and (2), the total energies of both Al and NaH and molecular H_2 were also computed with the same scheme.

Since the Kohn-Sham eigenvalues in the LDA or GGA approximation do not give the quasiparticle energies correctly, we use GW approximation to the many-body perturbation theory^{27,28} to provide corrections to the quasiparticle dispersion in these two hydrides. The cutoff energy was set to be 42 Ry, and a $4 \times 4 \times 4$ ($2 \times 2 \times 2$) Monkhorst-Pack grid is used for NaAlH_4 (Na_3AlH_6). To ensure the convergency of the calculation, we include 100 bands, which is more than 8–10 times of the number of valence bands. We calculated the static dielectric matrix within the random phase approximation (RPA) and use the generalized plasmon-pole model to extend the dielectric matrix to finite frequencies.²⁸

III. CRYSTAL STRUCTURE

NaAlH_4 crystallizes in a body-centered tetragonal structure having the $I4_1/a$ space group, while $\alpha\text{-Na}_3\text{AlH}_6$ has a monoclinic crystal structure with the $P2_1/n$ symmetry. The structures were confirmed by x-ray diffraction experiments^{11,12} and neutron scattering data for NaAlH(D)_4 ,¹³ and by a combined x-ray and neutron diffraction analysis for $\alpha\text{-Na}_3\text{AlH(D)}_6$.¹⁴ The crystal structures of NaAlH_4 and Na_3AlH_6 are illustrated in Fig. 1 where Al-H

TABLE I. Comparison between calculated (GGA) and experimental lattice constants and internal parameters for tetragonal NaAlH_4 (space group $I4_1/a$).

Lattice constants (\AA)	a	c	
	This work	5.09	11.39
Expt. ^a	5.021	11.346	
Expt. ^b	5.020	11.330	
Expt. (8 K) ^c	4.9802	11.1482	
Internal parameters	x	y	z
H (This work)	0.232	0.386	0.546
D (Exp. 8 K) ^c	0.2371	0.3867	0.5454

^aRef. 11.

^bRef. 12.

^cRef. 13.

bonds are drawn for clarity. Aluminum atoms are surrounded by four hydrogen atoms in NaAlH_4 and six in $\alpha\text{-Na}_3\text{AlH}_6$, forming the AlH_4 tetrahedral and AlH_6 octahedral complexes with an average Al-H bond length of 1.627 \AA (Ref. 13) and 1.758 \AA ,¹⁴ respectively. Both polyhedra show slight distortion from the ideal tetrahedral/octahedral geometry. There are two chemical units per primitive unit cell for both compounds. Starting from experimentally available parameters we have performed structural relaxations to optimize both the forces and stresses. The residual force and stress in the equilibrium geometry are of the order of 10^{-5} Ry/a.u. and 10^{-3} GPa, respectively.

The calculated GGA lattice parameters and internal parameters are listed in Tables I and II for NaAlH_4 and $\alpha\text{-Na}_3\text{AlH}_6$, respectively, together with the experimental values. The calculated lattice constants are 0.5–2.5 % larger than experimental values, which is typical for the GGA approximation to DFT. The internal parameters in our relaxed geometries compare well with the available neutron scattering data.^{13,14} In order to further assess the effects of the exchange-correlation approximation and the pseudopotentials, we have also studied structural properties of both compounds using the local density approximation (LDA) and tested the importance of the Al $3d$ nonlocal pseudopotential. Table III lists the percentage difference of the computed unit-cell volume using these different schemes compared with experimental values for both NaAlH_4 and $\alpha\text{-Na}_3\text{AlH}_6$. The explicit inclusion of the Al $3d$ nonlocal pseudopotential enhances the bonding and reduces the volumes by 2–3 % in every case. As will be shown later in Sec. IV, the Al $3d$ state does participate in the bonding in the AlH_6 complex and needs to be treated on equal footing as $3s$ and $3p$. GGA consistently yields a larger volume than experiment, while LDA consistently gives a smaller volume than GGA. We notice that GGA yields a better volume for NaAlH_4 , while the LDA volume is closer to experiment for $\alpha\text{-Na}_3\text{AlH}_4$.

IV. ELECTRONIC STRUCTURE

The energy band structure of NaAlH_4 is shown in Fig. 2. It exhibits a rather large energy gap of about 4.9 eV between

TABLE II. Comparison between calculated (GGA) and experimental lattice and internal parameters for monoclinic α -Na₃AlH₆ (space group $P2_1/n$). Lattice constants are in Å and angles in degrees.

Lattice parameters	<i>a</i>	<i>b</i>	<i>c</i>	β
This work	5.51	5.67	7.91	89.90
Expt. ^a	5.390	5.514	7.725	89.86
Internal parameters	<i>x</i>	<i>y</i>	<i>z</i>	
This work				
Na	-0.008	0.458	0.253	
H1	0.095	0.045	0.212	
H2	0.235	0.333	0.541	
H3	0.158	0.262	0.940	
Expt. ^a				
Na	-0.006	0.461	0.252	
D1	0.091	0.041	0.215	
D2	0.234	0.328	0.544	
D3	0.165	0.266	0.944	

^aRef. 14.

valence and conduction bands, indicating that the compound is a wide-gap insulator. This value is consistent with the previously reported GGA band gap of 5.04 eV (Ref. 7) and LDA band gap of 4 eV.⁶ To provide a more accurate description of the quasiparticle spectrum, we have also carried out a calculation of the self-energy correction using the many-body perturbation theory with the *GW* approximation which is particularly successful in predicting accurate values of energy band gaps for insulating materials.^{27,28} Fig. 3 shows the *GW* correction to the calculated GGA eigenvalues. The valence bands are shifted down by 1–2 eV to lower energies, while the conduction bands are shifted up by about 1 eV to higher energies. Therefore, the quasiparticle band gap is estimated to be about 6.9 eV.

The eight valence bands in Fig. 2 have a width of about 6 eV, and are split into two disjointed groups consisting of two and six bands, respectively. (Note that there are two chemical units and 16 valence electrons per unit cell.) These two groups do not overlap in energy and have a similar width of about 3 eV and an electron population ratio of 1:3. The

TABLE III. Percentage difference of the calculated unit-cell volume compared with experiment for different exchange-correlation and pseudopotential schemes. Potential *A* includes the Al *d* nonlocal potential explicitly, while potential *B* does not.

	Potential A		Potential B	
	GGA	LDA	GGA	LDA
NaAlH ₄	+2.8%	-7.6%	+5.9%	-4.6%
Na ₃ AlH ₆	+7.6%	+0.4%	+9.8%	+2.7%

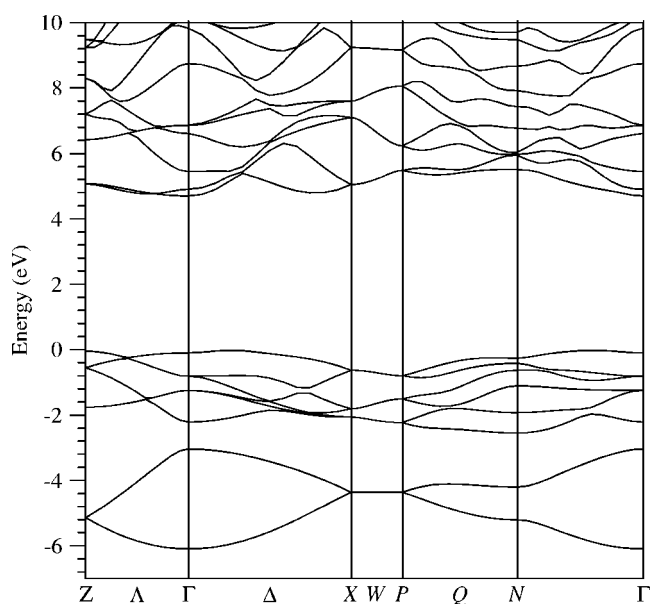


FIG. 2. Energy band structure of NaAlH₄. The energy zero is set at the top of the valence band.

band structure obtained in this pseudopotential calculation is in agreement with that from the LAPW calculation.⁶

A calculation of the total and projected density of states (DOS), shown in Fig. 4, reveals some interesting features. The angular-momentum projected DOS is evaluated by integrating over spheres centered at each atom with a radius of 1.5, 1.53, and 3.0 a.u. for H, Al, and Na, respectively. The choice of the H radius is made based on the charge distribution around H in order to catch the charge transfer to H. The radius of Al (1.53 a.u.) is then chosen according to the Al-H bond length, which may be too small to catch all the charge around Al, but the distribution of the angular-momentum decompositions should still provide valuable information. Finally the radius of Na is chosen to cover as much of the interstitial region as possible based on non-overlapping sphere.

It can be seen in Fig. 4 that the valence bands are dominated by H *s* contributions, while the conduction bands mainly by Na (and to lesser extent Al) empty states. Na has

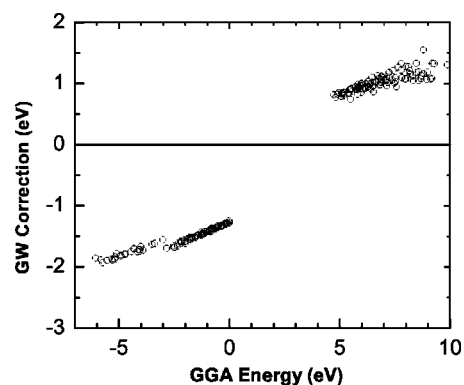


FIG. 3. Quasiparticle *GW* correction to the GGA energies for the band structure of NaAlH₄. Valence bands are shifted to a lower energy and conduction bands to a higher energy.

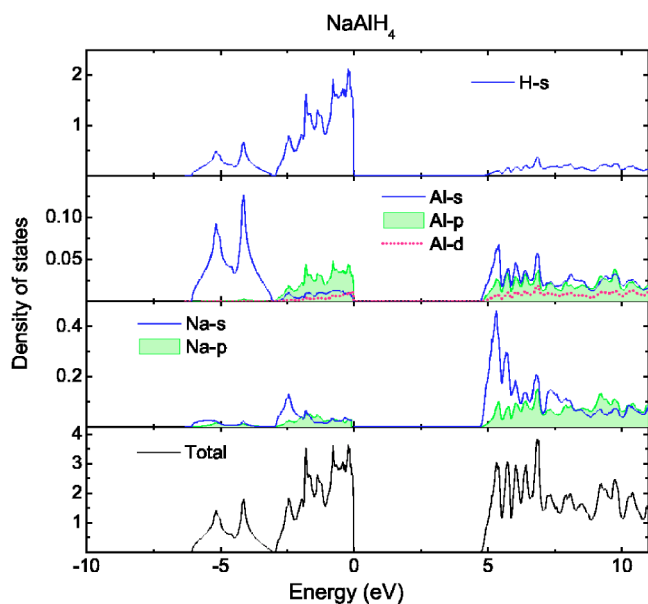


FIG. 4. (Color online) Electronic density of states and angular momentum projections for NaAlH_4 . The radius used to calculate the angular-momentum decomposed density of states is 1.5, 1.53, and 3.0 a.u. for H, Al, and Na, respectively.

hardly any projection in the occupied states, indicating the fact that it plays the role as an electron donor in the system. In comparison, H has hardly any projection in the range of the empty states shown in Fig. 4. The first two valence bands are derived from H s and Al s orbitals, while the next six bands in the higher-energy group are mainly from H s and Al p states. This does suggest that hybridization occurs between H and Al orbitals. However, the weighting of H s is considerably larger than those of Al s or p . These features point to a highly-ionic covalent bonding of hydrogen and aluminum in the anion complex AlH_4^- . This can be understood from the difference in the electron negativity for H and Al (2.1 versus 1.5). The ratio of 1:3 between the number of electrons hybridized with Al s and p is consistent with the tetragonal coordination in the complex.

The electronic structure can be further analyzed by examining the charge distribution and charge transfer in the AlH_4 complexes. We plot both the total charge density $\rho(\mathbf{r})$ and the difference charge densities $\rho_d(\mathbf{r})$ in the plane containing Al and H atoms of a single AlH_4 complex. The difference charge density $\rho_d(\mathbf{r})$ is defined as the difference between the total charge density of the solid and a superposition of atomic charge densities with the same spatial coordinates as in the solid, i.e.,

$$\rho_d(\mathbf{r}) = \rho(\mathbf{r}) - \sum_i \rho_{\text{atom}}^i(\mathbf{r} - \mathbf{R}_i), \quad (3)$$

where the sum is over all the atoms. Figure 5 shows such plots in the plane containing one Al and two neighboring H atoms in the AlH_4 complex. The buildup of the electron density at the H positions is clearly visible in the total charge density plot, while the difference density plot shows the charge transfer from Al to H leaving aluminum positively

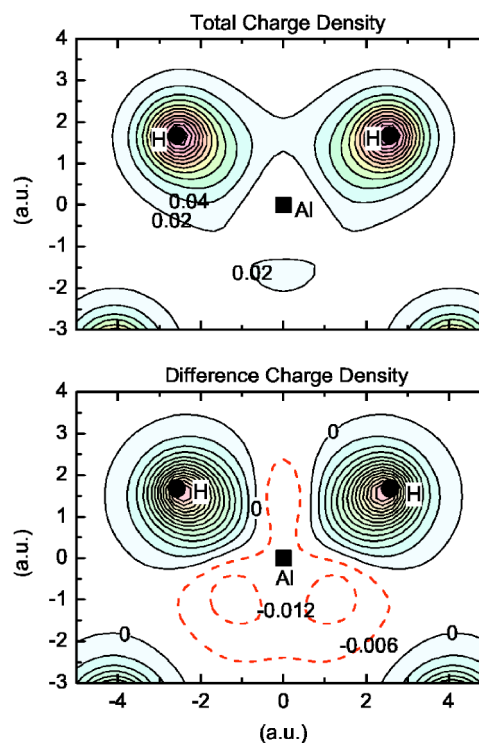


FIG. 5. (Color online) Total and difference charge-density plots of NaAlH_4 in a plane with Al and two H atoms. Top: The total charge density represented by contours in an interval of 0.02 electrons/(a.u.³). Bottom: Charge deficiency in the difference plot is plotted in dashed lines, while the density increase near the hydrogen atoms is plotted in solid lines with an increment of 0.006 electrons/(a.u.³) toward the hydrogen centers.

and hydrogen negatively charged. The charge density maximum near the H atoms is of the order of 0.26 electrons/(a.u.)³, while the maximum in the difference charge density plot is 0.09 electrons/(a.u.)³. It is noted that the zero charge density difference line forms a closed contour around H, leaving a large interstitial region with a negative density change. In other words, the deep proton potential easily attains electrons from the whole interstitial region. Moreover, the positive contours in the difference density plot is not exactly centered at the hydrogen site and is distorted toward Al, and the largest decrease in density near Al occurs in a region in the back of the Al-H bonds. These features support a covalent type of bonding but with a large ionicity.

The situation is similar to that of semiconductors with ionic covalent bonds. For the octet AB crystal family (e.g., GaAs, ZnSe, etc.) where the bonds are fully saturated, a connection has been established between the “charge transfer” and the structure. It has been recognized that with increasing charge transfer (measured by an ionicity scale), a transition exists from the fourfold coordinated structure, such as zinc blende and wurtzite, to the sixfold coordinated structure, such as rocksalt that is characterized by an ionic bonding.²⁹ In the AlH_4 complex considered here, a significant charge transfer is identified, but it is not large enough to destabilize the fourfold coordinated structure.

Based on these results the schematic representation of the bonding in the AlH_4^- unit is shown on the left-hand side of

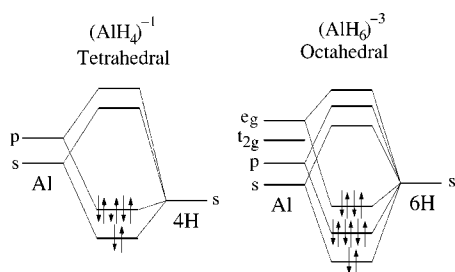


FIG. 6. Schematic representation of orbital hybridization and the occupation of bonding orbitals for both $(\text{AlH}_4)^-$ and $(\text{AlH}_6)^{-3}$ complexes.

Fig. 6. The Al 3s and 3p states hybridize with the H s state separately, forming two bonding states with a degeneracy of two and six, respectively. They are occupied by the eight valence electrons per AlH_4 complex. The covalent bonding is highly ionic, similar to that in, for example, II-VI semiconductors. The perfect sp^3 degeneracy is lifted, which is possibly responsible for the distortion of the tetrahedral AlH_4 complex away from a perfect tetrahedron. The ideal tetrahedron is characterized by a H-Al-H angle of 109.5° , while in the AlH_4 unit distortion yields two sets of angles of 107.3° and 113.9° ,¹³ respectively.

In comparison, Fig. 7 displays the energy band structure of $\alpha\text{-Na}_3\text{AlH}_6$ with a GGA band gap of 2.7 eV and a valence band consisting of three groups separated by finite gaps. The GW correction is shown in Fig. 8 where the top of the valence bands is shifted down by 1.0 eV, while the bottom of the conduction band is shifted up by 0.9 eV. This gives a final quasiparticle gap of 4.6 eV. The electronic DOS plots for these compound are shown in Fig. 9, including the angular-momentum decompositions with atomic radii chosen in a similar manner as in NaAlH_4 . The radius of the H sphere is again set to be 1.5 a.u. and the radius of the Al sphere is chosen to be 1.8 a.u. based on the Al-H bond length so that

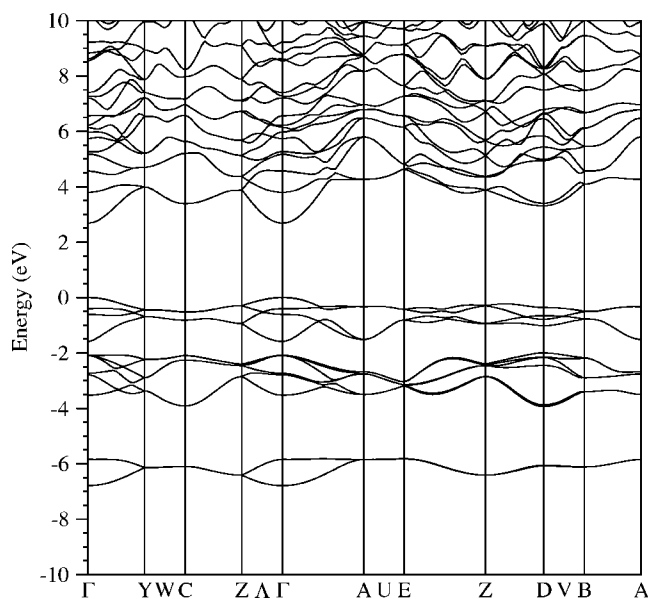


FIG. 7. Energy band structure of $\alpha\text{-Na}_3\text{AlH}_6$. The energy zero is set at the top of the valence band.

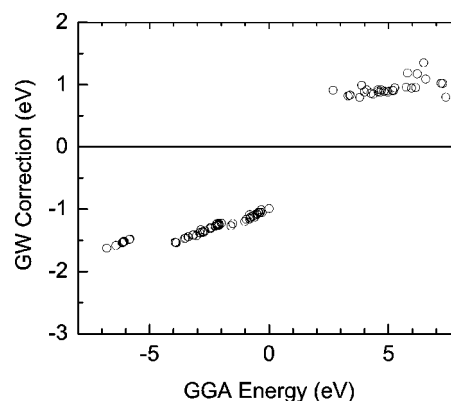


FIG. 8. Quasiparticle GW correction to the GGA energies for the band structure of Na_3AlH_6 . Valence bands are shifted to lower energy and conduction bands to higher energy.

the spheres do not overlap. Finally the radius of Na is chosen to be 2.7 a.u. in order to cover as much of the interstitial region as possible. Similar to NaAlH_4 , the valence band is predominantly H derived and conduction bands are mainly empty states associated with Na, indicating again a clear charge transfer.

For this compounds the valence band is split into three groups consisting of two, six, and four bands, respectively. (Note that there are two chemical units and 24 valence electrons per unit cell.) H s characteristics dominate in all of the three groups of valence states, which turn out to have distinctly different Al characteristics. It can be clearly seen in the decomposition around the Al site that the lowest-energy group is associated with Al s, the next one associated with Al p, and the top group associated with Al d, with a ratio of electron occupancy of 1:3:2. Therefore, one can understand

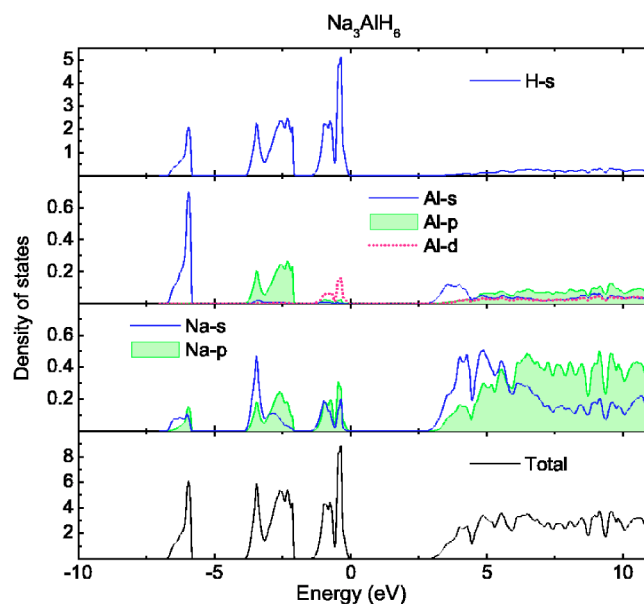


FIG. 9. (Color online) Electronic density of states and angular momentum projections for $\alpha\text{-Na}_3\text{AlH}_6$. The radius used to calculate the angular-momentum decomposed density of states is 1.5, 1.8, and 2.7 a.u. for H, Al, and Na, respectively.

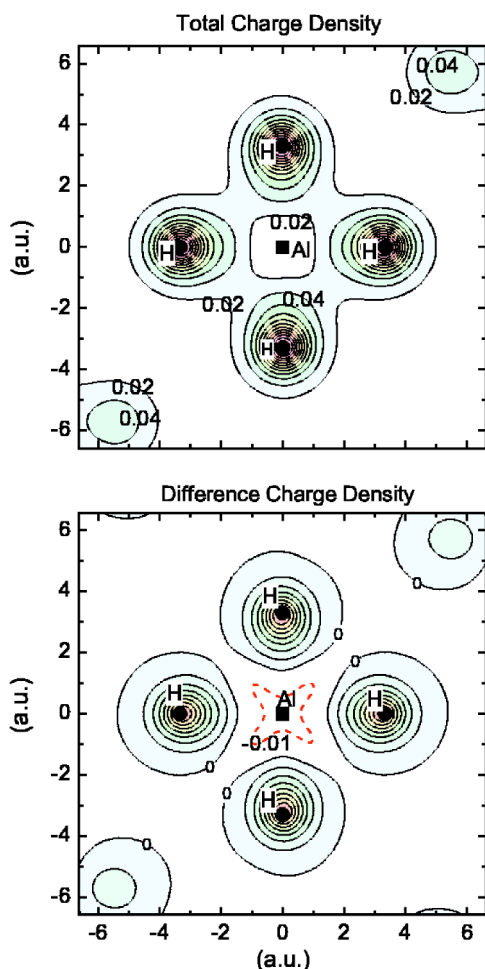


FIG. 10. (Color online) Total and difference charge-density plot of Na_3AlH_6 in the equatorial plane of the AlH_6 complex. Top: The total charge density represented by contours in an interval of 0.02 electrons/(a.u.)³. Bottom: Charge deficiency in the difference plot is plotted in dashed lines, while the density increase near the hydrogen atoms is plotted in solid lines with an increment of 0.01 electrons/(a.u.)³ toward the hydrogen centers.

the bonding within the complex based on the schematic diagram in Fig. 6. Within the AlH_6 octahedron with H ions sitting at the corners, the fivefold degeneracy of Al 3d orbitals will split, due to the crystal field effect, into a threefold t_{2g} and a twofold e_g orbitals. In the octahedral symmetry the e_g orbitals point directly from Al to the corner H atoms and could hybridize with H s orbitals, yielding a fully occupied bonding state. This interaction with Al d orbital was not considered in the analysis of the AlH_6 complex in the previous calculation of Li_3AlH_6 .¹⁶ In comparison, the BH_6 complex has never been observed. This octahedral configuration may not be favorable for B, because of the large energy difference between the 3d and 2s/p bonding states.

Figure 10 shows the electronic charge distribution of the octahedral AlH_6 complex in the equatorial plane consisting of Al and four H atoms. As in the tetrahedral AlH_4 complex discussed above, substantial electron gain at the hydrogen position also occurs in the AlH_6 complex. In both complexes Al is positively charged and surrounded by negatively

TABLE IV. Reaction energies for the dehydrogenation processes calculated for the relaxed structures in units of kJ/mol.

	This work	Expt.
$\text{NaAlH}_4 \rightarrow \frac{1}{3}\text{Na}_3\text{AlH}_6 + \frac{2}{3}\text{Al} + \text{H}_2$	31	36 ^a , 37 ^b
$\text{Na}_3\text{AlH}_6 \rightarrow 3\text{NaH} + \text{Al} + \frac{3}{2}\text{H}_2$	56	47 ^b
$\text{NaAlH}_4 \rightarrow \text{NaH} + \text{Al} + \frac{3}{2}\text{H}_2$	49	53 ^b

^aRef. 30.

^bRef. 31.

charged H, indicating a rather strong ionic character of the chemical bonding. The charge density maximum near the H atoms is about 0.26 electrons/(a.u.)³, and the maximum in the difference charge density plot is 0.09 electrons/(a.u.)³. Interestingly, these numbers are identical to those in NaAlH_4 . Close inspection of the difference charge plots of the hydrogen anions again shows slight distortion of the charge density contours from the circular shape. In fact the contours are somewhat elongated and have slightly more charge buildup along the Al-H direction, indicating the presence of orbital hybridization. From the difference charge plot, we do not find the covalent bonding between H atoms as suggested by Vajeeston *et al.*¹⁶

V. FORMATION ENERGY

Thermodynamic stability of complex hydrides NaAlH_4 and Na_3AlH_6 depends on its formation energy through reactions in Eqs. (1) and (2). These reaction energies calculated for the lowest-energy structures are summarized in Table IV, as well as the energy of a direct decomposition of NaAlH_4 to NaH metal hydride, Al metal, and H_2 gas. The energy of each species is calculated using the same pseudopotentials (potential A in Table III) and the same energy cutoff with GGA. The energy of a free H_2 molecule was computed in a large cubic cell of a 15 a.u. side length. NaH metal hydride and Al metal both crystallize in face-centered cubic structure and their respective $Fm-3m$ space group geometry was considered in energy calculations. The calculated total energies for the individual species are as follows: -23.9533 , -41.1650 , -4.1443 , -2.3294 , and -4.3006 Ry for 2NaAlH_4 , $2\text{Na}_3\text{AlH}_6$, Al, H_2 , NaH, respectively. It is expected that the error of these calculated results is of the order of 5–10 kJ/mol. The largest source of error in our calculation comes from the energy calculated for the hydrogen molecule H_2 where the density functional approach results are known to depart from the exact or measured value. The positive values in Table IV suggest endothermic dehydrating reactions which are not thermodynamically favorable at zero temperature and can be induced at elevated temperatures. The calculated result of 31 kJ/mol- H_2 for reaction (1) compares reasonably well with the experimental enthalpy of 36 kJ/mol obtained for undoped NaAlH_4 as described in Ref. 30. These results are also in good agreement with experimentally determined enthalpy changes of the reaction processes catalyzed by Ti, namely, 37 and 47 kJ/mol for reactions (1) and (2), respectively, and 53 kJ/mol for the direct decomposition of NaAlH_4 .³¹

VI. SUMMARY AND CONCLUSION

The structural, electronic and stability properties of NaAlH₄ and Na₃AlH₆ have been calculated and analyzed. Structural parameters including the lattice constants and internal parameters within the respective space groups were calculated and agree well with the experiment. The hydrogen positions in NaAlH₄ in particular are very close to the deuterium positions obtained in the neutron diffraction measurement at 8 K. The volume of the unit cell calculated with the GGA and LDA approximations with and without the explicit nonlocal Al-*d* pseudopotential shows a broad diapason of variations as high as ~10% of the experimental values. With the Al nonlocal *d* potential explicitly included in the calculation, the best calculated volume for NaAlH₄ is obtained with the GGA approach, while LDA gives a better unit-cell volume for Na₃AlH₆. Detailed calculations of electronic structure suggest that both complex hydrides are insulator with GGA energy band gaps of 4.9 and 2.7 eV for NaAlH₄ and Na₃AlH₆, respectively. The GW correction is evaluated for both complex hydrides and yield an increased band gap of 6.9 and 4.6 eV, respectively. The angular momentum projected electronic DOS as well as the charge density plots indicate significant charge transfer leading to Na⁺ ions and negatively charged AlH₄ and AlH₆ complexes. The charge

transfer from Al to H atom is similar in both AlH₄ and AlH₆ complexes. The bonding within the AlH₄ and AlH₆ complexes involves the hybridization between Al and H orbitals, but shows a strong ionic character. In the AlH₄ complex, Al *s* and *p* orbitals hybridize with the H *s* orbital, while in AlH₆ Al *d* orbitals split due to the crystal field effect and the *e_g* components also hybridize with Hs, leading to an additional group of bands. Total energy calculations are used to estimate the enthalpy change in the chemical reactions associated with the hydration/dehydration processes. The calculated values are in good agreement with measured values.

ACKNOWLEDGMENTS

We would like to thank Dr. C. M. Wei for technical assistance and Dr. K. Yvon for helpful discussions. This work is supported by the Department of Energy under Grant No. DE-FG02-97ER45632. A research grant from General Electric Global Research is gratefully acknowledged. The computation used resources of the National Energy Research Scientific Computing Center (NERSC), which is supported by the U.S. Department of Energy (Grant No. DE-AC03-76SF00098). We acknowledge the use of the PARATEC package at NERSC.

*Present address: Quantum Theory Project, University of Florida, Gainesville, Florida, 32611-8435.

¹A. Zuttel, *Mater. Today* **6**, 24 (2003).

²L. Schlapbach and A. Zuttel, *Nature* (London) **414**, 353 (2001).

³C. M. Jensen and K. J. Gross, *Appl. Phys. A: Mater. Sci. Process.* **72**, 213 (2001).

⁴K. J. Gross, G. J. Thomas, and C. M. Jensen, *J. Alloys Compd.* **330–332**, 683 (2002).

⁵B. Bogdanovic and M. Schwickardi, *J. Alloys Compd.* **253–254**, 1 (1997).

⁶A. Aguayo and D. J. Singh, *Phys. Rev. B* **69**, 155103 (2004).

⁷P. Vajeeston, P. Ravindran, R. Vidya, H. Fjellvag, and A. Kjekshus, *Appl. Phys. Lett.* **82**, 2257 (2003).

⁸S. M. Opalka and D. L. Anton, *J. Alloys Compd.* **356–357**, 486 (2003).

⁹M. E. Arroyo y de Dompablo and G. Ceder, *J. Alloys Compd.* **364**, 6 (2004).

¹⁰J. Iniguez, T. Yildirim, T. J. Udovic, E. H. Majzoub, M. Sulic, and C. M. Jensen, *Phys. Rev. B* **70**, 060101 (2004).

¹¹K. V. Belskii, B. M. Bulychev, and A. V. Golubeva, *Russ. J. Inorg. Chem.* **28**, 1528 (1983).

¹²J. W. Lauher, D. Dougherty, and P. J. Herley, *Acta Crystallogr., Sect. B: Struct. Crystallogr. Cryst. Chem.* **35**, 1454 (1979).

¹³B. C. Hauback, H. W. Brinks, C. M. Jensen, K. Murphy, and A. J. Maeland, *J. Alloys Compd.* **358**, 142 (2003).

¹⁴E. Rönnebro, D. Noréus, K. Kadir, A. Reiser, and B. Bogdanovic,

J. Alloys Compd. **299**, 101 (2000).

¹⁵P. Vajeeston, P. Ravindran, R. Vidya, H. Fjellvag, and A. Kjekshus, *Phys. Rev. B* **68**, 212101 (2003).

¹⁶P. Vajeeston, P. Ravindran, A. Kjekshus, and H. Fjellvag, *Phys. Rev. B* **69**, 020104 (2004).

¹⁷D. J. Singh (unpublished).

¹⁸P. Hohenberg and W. Kohn, *Phys. Rev.* **136**, B864 (1964).

¹⁹W. Kohn and L. Sham, *Phys. Rev.* **140**, A1133 (1965).

²⁰N. Troullier and J. L. Martins, *Phys. Rev. B* **43**, 1993 (1991).

²¹S. G. Louie, S. Froyen, and M. L. Cohen, *Phys. Rev. B* **26**, 1738 (1982).

²²Another Al pseudopotential with cutoff radii: 2.34(*s*), 2.20(*p*), and 2.28 a.u.(*d*) was also tested.

²³J. P. Perdew and Y. Wang, *Phys. Rev. Lett.* **66**, 508 (1991).

²⁴J. P. Perdew, K. Burke, and M. Ernzerhof, *Phys. Rev. Lett.* **77**, 3865 (1996).

²⁵D. M. Ceperley and B. J. Alder, *Phys. Rev. Lett.* **45**, 566 (1980).

²⁶H. J. Monkhorst and J. D. Pack, *Phys. Rev. B* **13**, 5188 (1976).

²⁷L. Hedin, *Phys. Rev.* **139**, A796 (1965).

²⁸M. S. Hybertsen and S. G. Louie, *Phys. Rev. B* **34**, 5390 (1986).

²⁹J. R. Chelikowsky and J. K. Burdett, *Phys. Rev. Lett.* **56**, 961 (1986).

³⁰C. M. Jensen and K. J. Gross, *Appl. Phys. A: Mater. Sci. Process.* **72**, 213 (2001).

³¹B. Bogdanović, R. A. Brand, A. Marjanović, M. Schwickardi, and J. Tölle, *J. Alloys Compd.* **302**, 36 (2000).